Diamagnetism of doped two-leg ladders and probing the nature of their commensurate phases

G. Roux,[1,*] E. Orignac,[2] S. R. White,[3] and D. Poilblanc[1]
[1]*Laboratoire de Physique Théorique, IRSAMC, Université Paul Sabatier, CNRS UMR5152, 118 Route de Narbonne, 31400 Toulouse, France*
[2]*Laboratoire de Physique de l'École Normale Supérieure de Lyon, ENS-Lyon, CNRS UMR5672, 46 Allée d'Italie, 69007 Lyon, France*
[3]*Department of Physics and Astronomy, University of California, Irvine, California 92697, USA*
(Received 19 July 2007; revised manuscript received 21 September 2007; published 2 November 2007)

We study the magnetic orbital effect of a doped two-leg ladder in the presence of a magnetic field component perpendicular to the ladder plane. Combining both low-energy approach (bosonization) and numerical simulations (density-matrix renormalization group) on the strong coupling limit (t-J model), a rich phase diagram is established as a function of hole doping and magnetic flux. Above a critical flux, the spin gap is destroyed and a Luttinger liquid phase is stabilized. Above a second critical flux, a reentrance of the spin gap at high magnetic flux is found. Interestingly, the phase transitions are associated with a change of sign of the orbital susceptibility. Focusing on the small magnetic field regime, the spin-gapped superconducting phase is robust, but immediately acquires algebraic transverse (i.e., along rungs) current correlations which are commensurate with the $4k_F$ density correlations. In addition, we have computed the zero-field orbital susceptibility for a large range of doping and interaction ratio J/t: we found strong anomalies at low J/t only in the vicinity of the commensurate fillings corresponding to $\delta=1/4$ and $1/2$. Furthermore, the behavior of the orbital susceptibility reveals that the nature of these insulating phases is different: while for $\delta=1/4$ a $4k_F$ charge density wave is confirmed, the $\delta=1/2$ phase is shown to be a bond order wave.

DOI: 10.1103/PhysRevB.76.195105 PACS number(s): 74.20.Mn, 71.10.Pm, 75.40.Mg, 75.20.−g

I. INTRODUCTION

Ladder systems have proven to be remarkably interesting systems, both as simple models exhibiting behavior similar to two-dimensional (2D) systems, and as systems exhibiting competition between several types of ground states. Theoretical models of doped ladders display a large superconducting (SC) phase[1–6] with d-wave pairing associated with the presence of a spin gap, with a ground state which can be described variationally as a short-ranged resonating valence bond state.[7] Charge density wave (CDW) correlations compete with the pairing correlations.[5,6,8,9] The phase diagram of the isotropic t-J model was sketched in Ref. 6 and displays, in addition to this competition, insulating phases for the particular commensurate dopings $\delta=1/4$ and $1/2$. Another competition exists between the superconducting phase and an orbital antiferromagnetic flux (OAF) phase,[5,10–14] which has been addressed in different ladder models by studying transverse current correlations which display a quasi-long-range order in the OAF phase.

Ladders are also among the simplest systems through which a magnetic flux can pass (see Fig. 1). When a magnetic field H is applied to an electronic system, it couples to both the spin of the electron, via Zeeman effect, and to the charge degree of freedom, via orbital effect. The total magnetic susceptibility of a real material splits into various contributions[15] $\chi=\chi^{\mathrm{spin}}+\chi^{\mathrm{orb}}_{\mathrm{cond}}+\chi^{\mathrm{orb}}_{\mathrm{core}}$, where χ^{spin} is the Pauli susceptibility, and $\chi^{\mathrm{orb}}_{\mathrm{cond}}$ and $\chi^{\mathrm{orb}}_{\mathrm{core}}$ are the orbital susceptibilities of the conduction and core electrons. $\chi^{\mathrm{orb}}_{\mathrm{core}}$ must be evaluated from local atomic orbital, and we will neglect it in what follows. $\chi^{\mathrm{orb}}_{\mathrm{cond}}$ is usually difficult to evaluate because one has to precisely describe the evolution of the whole band structure with magnetic field.[16,17] In the following, we will investigate $\chi^{\mathrm{orb}}_{\mathrm{cond}}$ within a single-orbital model. When the magnetic field is applied parallel to the plane of the ladder, the orbital effect is suppressed and only the Zeeman effect remains. The latter case has been discussed in detail in this system, and it was shown that a doping-controlled magnetization plateau and a large Fulde-Ferrell-Larkin-Ovchinnikov phase are obtained.[18–20] Since the ladder possesses a spin gap, when the magnetic field is not in the ladder plane, the orbital contribution may dominate the spin contribution in the total susceptibility at low temperature.

Early numerical investigations of the t-J model with magnetic orbital effect on ladders and 2D lattices revealed a strong effect of the magnetic field on the magnetic and pairing properties,[21] but the results were limited to small systems. A bosonization study of a related model of spinless fermionic ladders suggested the possibility of fractional excitations and of an OAF phase induced by the magnetic field.[22,23] Carr and Tsvelik[9] studied the orbital effect of the magnetic field on the interladder coupling using an effective model to describe a single ladder. Lastly, it has been predicted[24] that bosonic ladders could have commensurate

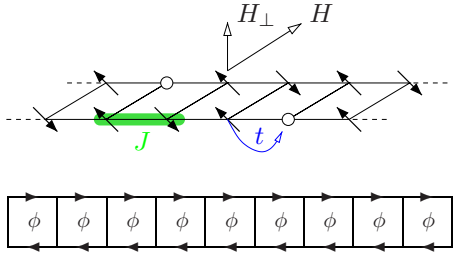

FIG. 1. (Color online) The isotropic t-J ladder under a magnetic field. If the magnetic field has a component perpendicular to the ladder plane, a flux ϕ passes through each plaquette. Below is the gauge of the Peierls substitution with opposite phases $\pm\phi/2$ along the legs.

vortex phases at commensurate fluxes, which would represent a one-dimensional analog of the two-dimensional vortex phase.

The purpose of the present paper is to consider the effect of a nonzero flux on the magnetic susceptibility on a single two-leg ladder, and also to investigate the effect of stronger fluxes on the zero temperature phase diagram of the ladder. To this end, we combine the bosonization technique and density-matrix renormalization group[25–27] (DMRG; see Appendix B for details) to compute the phase diagram and physical properties of a spin-1/2 fermionic ladder with orbital effect. The results are presented in two parts. The first part is devoted to the analysis of the phase diagrams as a function of the flux ϕ per plaquette in the weak- and strong-coupling limits. The second part is focused on the physics of the spin-gapped phase of a doped ladder at small flux, which is more relevant to realistic magnetic fields. In particular, we discuss the stability of the insulating phases at $\delta=1/4$ and $1/2$ present in the phase diagram of the t-J model at zero flux. In the Conclusion, we briefly give considerations to experiments which are connected to these results. For sake of clarity, we have relegated some of the technical details to the appendixes.

Including the flux

The magnetic flux couples to the kinetic part of the Hamiltonian through Peierls substitution.[17,28,29] In what follows, different hopping amplitudes along the chains ($t_\parallel$) and between the chains ($t_\perp$) are considered, and the Hamiltonian is

$$\begin{aligned}\mathcal{H}_t = &- t_\parallel \sum_{i,\sigma} [e^{i\phi/2} c^\dagger_{i+1,1,\sigma} c_{i,1,\sigma} + \text{H.c.}] \\ &- t_\parallel \sum_{i,\sigma} [e^{-i\phi/2} c^\dagger_{i+1,2,\sigma} c_{i,2,\sigma} + \text{H.c.}] \\ &- t_\perp \sum_{i,\sigma} [c^\dagger_{i,2,\sigma} c_{i,1,\sigma} + \text{H.c.}],\end{aligned} \tag{1}$$

where $c_{i,l,\sigma}$ is the electron creation operator at site i on leg l with spin σ. ϕ denotes the dimensionless flux per plaquette

$$\phi = \frac{e}{\hbar} \oint_\square A(x) dx = \frac{e}{\hbar} H_\perp a^2, \tag{2}$$

with $A(x)$ the vector potential which depends on the gauge choice, and a the lattice spacing. The magnetic field breaks time-reversal and chain exchange symmetries, which, as expected, will have notable consequences on the current properties of the system. Symmetry and periodicity considerations allow us to limit the study to flux $0 \leqslant \phi \leqslant \pi$. Exchanging chains amounts to reversing the direction of the magnetic field. More details on the gauge and flux quantization on finite systems can be found in Appendix B. The unit of ϕ is $2\pi\phi_0$, with $\phi_0 = h/e = 4.1357 \times 10^{-15}$ T m^2. For experimental considerations, a flux $\phi = 0.01\pi$ already corresponds to a very high magnetic field of $H \sim 800$ T for a typical value $a = 4$ Å of the Cu-O-Cu bond in a cuprate. The gauge chosen in Eq. (1) is represented in Fig. 1.

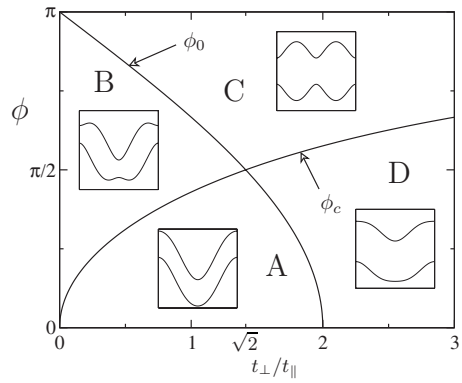

FIG. 2. The four typical shapes of the bands depending on the flux and on the ratio $t_\perp/t_\parallel$. Critical fields ϕ_0 (ϕ_c) signal the appearance of a double well (band gap). Note that the D phase always has only two Fermi points whatever the filling, and that the C phase *when* $\phi=\pi$ always has four Fermi points.

II. PHASE DIAGRAMS

A. Weak-coupling limit

We first introduce interactions between electrons using the Hubbard ladder in a magnetic flux. The Hamiltonian comprises the kinetic term $\mathcal{H}_t$ incorporating the flux and the on-site repulsion $U>0$:

$$\mathcal{H} = \mathcal{H}_t + U \sum_{i,p} n_{i,p,\uparrow} n_{i,p,\downarrow}. \tag{3}$$

According to the usual strategy,[5] we will consider, first, the limit $U=0$ and study the noninteracting band structure. Then, we will turn on $U \ll t_\parallel, t_\perp$ so that the band structure is not deformed, and obtain the different phases in this weak-coupling limit. Let us begin with the discussion of the band structure.

The magnetic flux has a strong effect on the shape of the bands. Indeed, it mixes the bonding (0) and antibonding (π) bands which exist at zero flux. To emphasize the difference with the zero-field case, we call the two bands obtained at finite flux the down (d) and up (u) bands. Results on the band structure are discussed in Refs. 22 and 23, and extended to a finite and fixed filling in Appendix A. The band structure depends on the flux ϕ and on the ratio $t_\perp/t_\parallel$ (see Fig. 2). We define two characteristic fluxes ϕ_c and ϕ_o, both of them dependent on $t_\perp/t_\parallel$, such that above ϕ_c, a double well appears in both bands, and above ϕ_0, a band gap opens between the bands u and d. Four different possible shapes of the bands are obtained according to the location of the flux with respect to ϕ_c and ϕ_o. The two critical flux lines crosses at $(t_\perp/t_\parallel = \sqrt{2}, \phi = \pi/2)$. By filling these bands, one can show (see Appendix A) that only situations with either two or four Fermi points can occur. The location of these Fermi points and their respective Fermi velocities vary continuously with the flux. In the rest of the paper, we will work only at fixed electronic density (denoted by n), which will constrain the sum of the Fermi momenta as a result of the Luttinger theorem.[30]

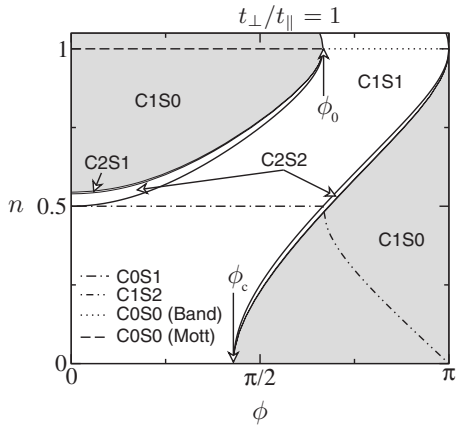

FIG. 3. Phase diagram in the weak-coupling limit for an isotropic ladder restricted to fillings $0 \leqslant n \leqslant 1$. Phases with four (two) Fermi points fall generically into the C1S0 (C1S1) class. At half-filling, interactions will drive the system into a Mott insulating phase for $\phi < \phi_0$, while a band insulating phase occurs when $\phi > \phi_c$. Other phases can be found if the ratio of the Fermi velocity is large (C2S1 and C2S2) and if the d-band Fermi wave vector is $\pi/2$ (C0S1 and C1S2).

Having obtained the noninteracting band structure, we add interactions small enough not to perturb the band structure, following the strategy of Refs. 4 and 31–34. Adopting the usual notation CpSq for a phase with p gapless charge modes and q gapless spin modes, a system with two Fermi points and repulsive interactions is expected to be generically in a C1S1 phase, i.e., a Luttinger liquid state. With four Fermi points and repulsive interactions, the system is generically in a C1S0 phase, i.e., a Luther-Emery liquid, which is the universality class of usual doped two-leg ladders. The critical fields at which the system changes from four to two or from two to four Fermi points can be computed analytically (see Appendix A). Note that from Refs. 4, 33, and 34, in the case of four Fermi points, other phases such as C2S1 or C2S2 appear when the difference between the two Fermi velocities becomes sufficiently large to prevent runaway of some coupling constants in the renormalization group flow. The large velocity difference implies that these phases are in the vicinity of the transition region between the C1S0 and C1S1 phases, where the Fermi velocity of the band that is emptying is going to zero. Moreover, this also implies that both the C2S1 and C2S2 phases have a very small extent near the transition region.[4,33,34] The above considerations apply for a system at a generic incommensurate filling. At commensurate filling, umklapp interactions can be relevant and lower the number of gapless modes.[4,33,34] More specifically, at half-filling, an insulating phase C0S0 of the Mott type (band type) is expected for $\phi < \phi_0$ ($\phi > \phi_0$). It is also possible to have an umklapp interaction inside the bonding band (if its Fermi wave vector equals $\pi/2$) leading to either a C0S1 or a C1S2 phase.[4] The phase diagram of an isotropic ladder resulting from these considerations is given in Fig. 3, where the main feature is a reentrance of the C1S0 phase at high flux. The high flux C1S0 phase has a band structure very similar to the one of the Hubbard chain, with a next-nearest hopping term[35,36] t' for $t' \gtrsim t/2$ and the same competing orders as the low flux C1S0 phase as we will see. This phase diagram is generic for $t_\perp/t_\parallel < 2$ except that $\phi_0 < \phi_c$ when $t_\perp/t_\parallel > \sqrt{2}$. For $t_\perp/t_\parallel > 2$, the C1S0 phase at low flux around half-filling disappears.

B. Strong-coupling limit: Numerical results on the t-J model

We now let the interactions go to the strong-coupling regime $U \gg t$, where the Hubbard model (3) reduces to the t-J model with $J \simeq 4t^2/U$. In this limit, we only use isotropic couplings $t = t_\parallel = t_\perp$ and $J = J_\parallel = J_\perp$ so that the t-J Hamiltonian simply reads

$$\mathcal{H}_{t-J} = \mathcal{P}\mathcal{H}_t\mathcal{P} + J\sum_{\langle i,j\rangle}\left[\mathbf{S}_i \cdot \mathbf{S}_j - \frac{1}{4}n_i n_j\right], \tag{4}$$

where $\mathbf{S}_i$ is the spin operator and $n_i = c_{i,\sigma}^\dagger c_{i,\sigma}$ is the electronic density operator (leg index is omitted in $\mathbf{S}_i$ and n_i). $\mathcal{P}$ is the Gutzwiller projector, which prevents double occupancy on a site. Observables are computed with DMRG for the range of doping $0 < \delta = 1 - n < 0.5$. The phase diagram will be discussed for the special case $J/t = 0.5$, for which the system has dominant superconducting fluctuations.[2,6]

1. Orbital susceptibility

The results for the noninteracting system of Appendix A show that the orbital susceptibility plotted in Fig. 15 changes sign at the transitions from $4 \leftrightarrow 2$ Fermi points with sharp discontinuities (for $0 < \delta < 0.5$). It is important to note that the noninteracting orbital susceptibility contains contributions from all the occupied states and not just those at the Fermi level which control the low-energy properties. Therefore, such connection between the change of sign of the orbital susceptibility and the change in the number of Fermi point is not obvious. Nevertheless, we propose to extend this way of probing the phase diagram to the interacting situation. Indeed, we can compute the screening current $j_\parallel$ and its associated susceptibility χ^{orb} as a function of the flux ϕ using the definitions

$$j_\parallel(\phi) = -\frac{1}{L}\frac{\partial E_0}{\partial \phi} \quad \text{and} \quad \chi^{\text{orb}}(\phi) = -\frac{1}{L}\frac{\partial^2 E_0}{\partial \phi^2}, \tag{5}$$

in which $E_0(\phi)$ is the ground-state energy and L is the length of the ladder. With this definition, $\chi^{\text{orb}}(\phi) > 0$ corresponds to orbital diamagnetism. The first relation is a consequence of the Feynman-Hellman theorem, and the second one results from the definition of the susceptibility as $\partial j_\parallel/\partial\phi$. This screening current can be related to the mean value of the current operators $j_{1,2}$ along the two chains by noting that $j_\parallel(\phi) = \langle j_2 - j_1\rangle/2$. Numerically, these quantities are computed directly from centered energy differences (to minimize discretization effects)

$$j_\parallel(\phi) = -[E_0(\phi + d\phi) - E_0(\phi - d\phi)]/2Ld\phi, \tag{6}$$

$$\chi^{\text{orb}}(\phi) = [j_\parallel(\phi + d\phi) - j_\parallel(\phi - d\phi)]/2d\phi, \tag{7}$$

using the conditions $j_\parallel(0) = j_\parallel(\pi) = 0$ (see Appendix B) and the right and left derivatives for $\chi^{\text{orb}}(0)$ and $\chi^{\text{orb}}(\pi)$. These

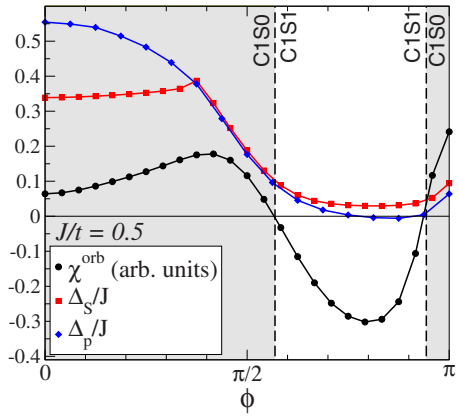

FIG. 4. (Color online) Orbital susceptibility, charge, and spin gaps for $J/t=0.5$ and on the $\delta=0.063$ line of Fig. 5. The zeros of the susceptibility precisely probe the different two phase transitions.

quantities are easy to compute numerically and are found to have small finite size effects for $J/t=0.5$. The effect of interactions is to smooth the discontinuities at the transitions, but we still expect that the sign changes of the susceptibility do correspond to transitions between C1S0 and C1S1 phases even in the strong-coupling limit (see Fig. 4). The phase diagram obtained from this ansatz is consistent with the behavior of other observables such as spin-spin correlation functions as will be seen in the next paragraphs. Thus, we can sketch in Fig. 5 a phase diagram similar to that of Fig. 3 for the t-J model with $J/t=0.5$. Compared with the weak-coupling phase diagram, the C1S1 phase is slightly wider at low doping, but thinner for $\delta \simeq 0.5$. Even in the presence of strong interactions, the overall shape of the phase diagram is not affected (although the precise location of the phase boundaries in the δ, ϕ plane does depend on U/t or J/t). Hence, for typical densities $0.5<n<1$ in the isotropic t-J model, the leading effect which governs the phase diagram is the change of the band structure under the applied flux. Lastly, one must note that the C1S0 phase persists at small flux at quarter-filling, $\delta=n=0.5$, in contrast to Fig. 3. This

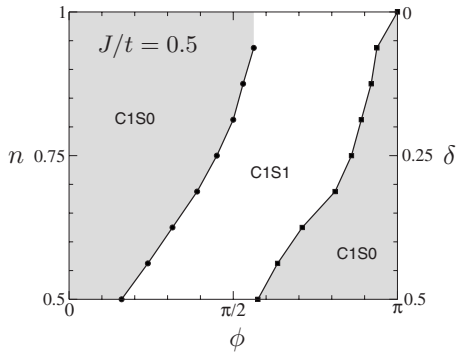

FIG. 5. Phase diagram of the t-J model for $J/t=0.5$, for which the system has dominant superconducting fluctuations at zero flux, determined from the zeros of the susceptibility on a system with $L=32$. Results are very similar to Fig. 3, with a transition to a C1S1 phase at intermediate flux and a reentrance to a C1S0 phase at large flux.

can be qualitatively explained by noting that renormalization group studies on coupled chains have shown that interactions reduce the interchain hopping integral $t_\perp$ with respect to its noninteracting value.[37,38]

2. Elementary excitations: Pairing energy and spin gap

The elementary excitations of a doped two-leg ladder are either the creation of a magnon, the cost of which is the spin gap Δ_S, or the creation of two quasiparticles by breaking a Cooper pair, the cost of which defines the pairing energy Δ_p. Following Refs. 20 and 39, we compute them numerically from the definitions

$$\Delta_S = E_0(n_h, S^z = 1) - E_0(n_h, S^z = 0), \tag{8}$$

$$\Delta_p = 2E_0(n_h - 1, S^z = 1/2) - E_0(n_h, S^z = 0) - E_0(n_h - 2, S^z = 0), \tag{9}$$

with $E_0(n_h, S^z)$ the ground-state energy of a system with n_h holes and spin S^z along the z axis. Since one can always have a $S^z=1$ state by breaking a Cooper pair, the condition $\Delta_S < \Delta_p$ must be satisfied in the thermodynamic limit. For $\phi=0$ and $J/t=0.5$, it is known[39] that the pair-breaking excitation is larger than the magnon excitation (lowest triplet excitation). These elementary gaps as a function of the flux are displayed in Fig. 4. We observe a decrease of the pairing energy with ϕ toward 0 at the critical flux corresponding to the onset of the C1S1 phase. In the C1S1 phase, we have a metallic Luttinger liquid phase with zero pairing energy. The cancellation of the pairing energy is, thus, the result of a band emptying mechanism and should not be confused with a magnetic superconducting critical field H_{c2}, which would correspond to a high density of vortices in a 2D (albeit anisotropic) superconducting material. Indeed, we do not observe a H_{c1} superconducting critical field or commensurate vortex phases as in the model of a bosonic ladder of Ref. 24. A situation corresponding to a true H_{c2} critical field might rather be a small flux through an array of coupled ladder. In this respect, the approach of Ref. 9 computes correctly the H_{c2} field up to a few approximations.

The spin gap increases at low magnetic field until it crosses Δ_p (see Fig. 4). From local hole densities (data not shown), the domain of hole pairs slightly shrinks, which can be interpreted as a reinforcement of the spin-liquid background at a low magnetic field, in agreement with exact diagonalization results previously discussed.[21] For a larger flux but still in the C1S0 phase, the spin gap Δ_S becomes identical to the pairing energy Δ_p, and both decrease toward zero as the flux is increased. The energy difference $\Delta_p - \Delta_S$ can be interpreted as the energy of a bound state of a magnon and a hole pair. This magnetic resonant mode was discussed previously at zero flux by varying interactions,[39–41] and its origin was related to the opening of doping-controlled magnetization plateaus.[19,20] Thus, the effect of adding Zeeman coupling at low flux ($\phi \lesssim \pi/3$ for $J/t=0.5$) would give very similar results to those of Refs. 19 and 20 since the bound state survives in a rather high magnetic flux. Finally, a small spin gap is recovered at high flux (near $\phi=\pi$), in agreement with the weak-coupling limit predictions.

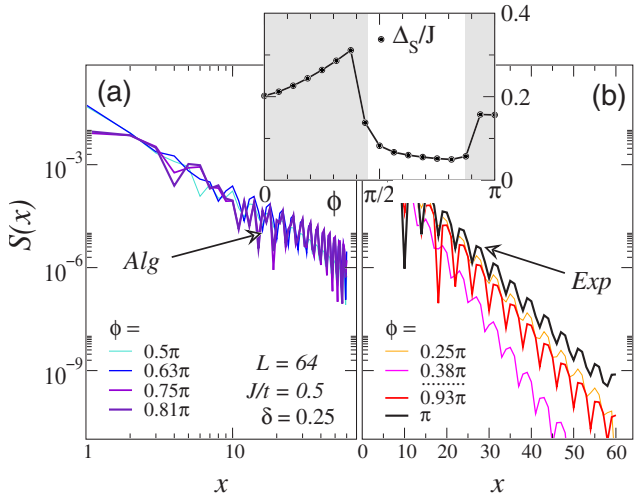

FIG. 6. (Color online) Spin correlations $S(x)$ for fluxes (a) in the C1S1 phase and (b) in the C1S0 phases at low and high fluxes in the phase diagram of Fig. 5 on the δ=0.25 line. Inset: The behavior of the spin gap computed on the same system using Eq. (8). These independent observables confirm the reentrance of the C1S0 phase.

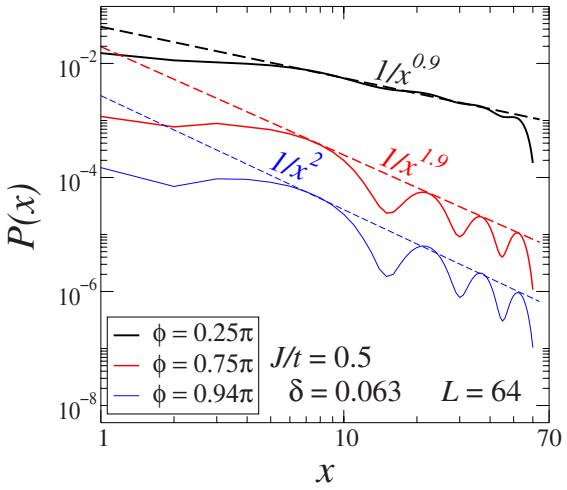

FIG. 7. (Color online) Superconducting correlations $P(x)$ for three values of the flux corresponding to each phase encountered on the δ=0.063 line of the phase diagram of Fig. 5. The decrease exponent is much higher in the C1S1 and high-flux C1S0 phases, and the overall magnitude is strongly reduced, suggesting a metallic state. Note that correlations display oscillations associated with a $4k_F$ contribution.

To gain further insights on these excitations, we have computed the spin and pair correlation functions in the ground state. The spin correlations $S(x)=\langle \mathbf{S}(x)\cdot\mathbf{S}(0)\rangle$ are short range in a spin-gapped phase with a correlation length $\xi\sim 1/\Delta_S$, which gives a complementary estimation of the evolution of the spin gap, particularly important when the pairing energy is smaller than the spin gap. From Fig. 6, we find a similar increase of the spin gap (smaller ξ) at small flux and algebraic correlations in the C1S1 phase. The spin gap at high flux is again recovered with short-range spin correlations.

The singlet operators on a rung defined by $\Delta(x)=c_{x,1,\uparrow}c_{x,2,\downarrow}-c_{x,1,\downarrow}c_{x,2,\uparrow}$ give the pairing correlations $P(x)=\langle\Delta(x)\Delta^{\dagger}(0)\rangle$. While $P(x)$ remains algebraic in the C1S0 and C1S1 phases, its overall magnitude follows the pairing energy and is strongly reduced in the C1S1 phase. These correlations can be discussed from the bosonization approach using the conventions and definitions of Appendix C. We find that the low-energy dominant term at wave vector $q=0$ in the low-field C1S0 phase reads

$$\Delta(x) \propto \sum_{\sigma} \sigma[(a_d)^2\psi_{d,R,\sigma}\psi_{d,L,-\sigma} + (b_d)^2\psi_{d,L,\sigma}\psi_{d,R,-\sigma} - (b_u)^2\psi_{u,R,\sigma}\psi_{u,L,-\sigma} - (a_u)^2\psi_{u,L,\sigma}\psi_{u,R,-\sigma}].$$

For instance, the intraband terms read

$$\psi_{p,R,\sigma}\psi_{p,L,-\sigma} \sim e^{i[\theta_{c+}+p\theta_{c-}-\sigma(\phi_{s+}+p\phi_{s-})]}, \tag{10}$$

with $p=\pm$ for d/u. From previous results,[5] we know that in a C1S0 phase, all the fields except ϕ_{c+} are gapped, with $\langle\theta_{c-}\rangle=0$ and $\langle\phi_{s+}\rangle=\pi/2$, $\langle\phi_{s-}\rangle=\pi/2$. These terms are, thus, algebraic with a decay exponent $1/2K_{c+}$, which is the continuation of the zero-flux physics. We observe from Fig. 7 that K_{c+} increases with the magnetic field, but a precise evaluation is numerically difficult.

In the C1S1 phase, superconducting correlations are expected and found to be algebraic with an exponent $K_c^{-1}+K_s$, but with a much smaller amplitude, in agreement with a metallic phase.

The physical properties of the high-flux C1S0 phase are very similar to those of the low-field C1S0 phase. Following the analysis by Fabrizio[35] (see Appendix C for notation), the pairing order parameter in this phase reads

$$\Delta(x) \propto \sum_{\sigma} \sigma[(a_1)^2\psi_{1,R,\sigma}\psi_{1,L,-\sigma} + (b_1)^2\psi_{1,L,\sigma}\psi_{1,R,-\sigma} + (b_2)^2\psi_{2,R,\sigma}\psi_{2,L,-\sigma} + (a_2)^2\psi_{2,L,\sigma}\psi_{2,R,-\sigma}],$$

which will give fluctuations with an exponent $1/2K_{c+}$. Computing the density and transverse current order parameters shows that they have a $2K_{c+}$ decay exponent associated with the wave vector $2(k_{F,1}-k_{F,2})=2\pi n$. The competing orders are, thus, the same as in the low-field phase studied in Sec. III. The fact that the SC signal is small and with a large exponent in Fig. 7 suggests that the CDW fluctuations dominate in this strong-coupling regime, making the high-flux C1S0 phase a spin-gapped metallic phase with strong transverse current fluctuations.

III. LOW-FIELD PROPERTIES OF THE LUTHER-EMERY PHASE

This section discusses the properties of the C1S0 Luther-Emery phase at very low fluxes relevant to the experimental accessible magnetic fields.

A. Current densities and correlations

With open boundary conditions used in DMRG, we have access to the local density of holes and currents. The local

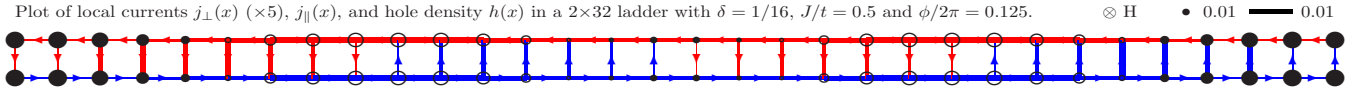

FIG. 8. (Color online) Local hole density and local currents in the ground state of the C1S0 phase (at low flux). The area of the circles is proportional to $h(x)-\delta$, with $h(x)$ the local density of holes. An excess of hole is represented by empty circles, while a lack of holes is represented by full circles. The line thickness is proportional to the current strength, and the arrow gives the direction. Note that the transverse current has been rescaled [by a factor (×5)]; the main screening currents are on the chains. Interestingly, the orbits have a length scale δ^{-1} determined by the average hole density.

hole density reads $h(x)=1-\langle n(x)\rangle$, while the mean values of local parallel and transverse current operators are computed using the definitions

$$j_\parallel^1(x) = it_\parallel[e^{i\phi/2}c_{x+1,1,\sigma}^\dagger c_{x,1,\sigma} - e^{-i\phi/2}c_{x,1,\sigma}^\dagger c_{x+1,1,\sigma}],$$

$$j_\parallel^2(x) = it_\parallel[e^{-i\phi/2}c_{x+1,2,\sigma}^\dagger c_{x,2,\sigma} - e^{i\phi/2}c_{x,2,\sigma}^\dagger c_{x+1,2,\sigma}],$$

$$j_\perp(x) = it_\perp[c_{x,1,\sigma}^\dagger c_{x,2,\sigma} - c_{x,2,\sigma}^\dagger c_{x,1,\sigma}]. \quad (11)$$

They are related to the current operator j_p along the chain p via $j_p=\frac{1}{L}\Sigma_x j_\parallel^p(x)$, and thus, to the screening current $j_\parallel(\phi)$. We have checked that Kirchhoff's conservation law for charge currents is satisfied at each vertex of the lattice. At zero flux, no currents are present in the ladder. When the magnetic field is applied, time-reversal symmetry is broken and local currents have a nonzero expectation value, depicted in Fig. 8 for a 2×32 ladder with four holes. First, the two hole pairs manifest themselves by two domains (areas with open circles). The local screening currents develop inside these domains and not at the edges of the ladder. Clearly, in the strong-coupling limit where double occupancy is prohibited, the only domains in which electrons can take advantage of the flux are the room left by holes. This results in a periodic pattern for hole currents whose length scale is exactly δ^{-1} (=16 in Fig. 8). Such a length scale is different from the usual magnetic length $\sqrt{\hbar/eH}$ governing orbits of Landau levels. A similar length scale has been found in the study of OAF phases,[14] while the current pattern is different from the one observed under a magnetic field. Note that these diamagnetic currents are not related to the Meissner effect expected in a superconductor or in a bosonic ladder.[24] Actually, hole pairs are delocalized on the two chains so that this pattern does not correspond to currents *of* pairs but rather to currents *inside* pairs.

To study the nature of the current fluctuations, we have computed the transverse current correlations

$$J(x) = \langle j_\perp(x)j_\perp(0)\rangle - \langle j_\perp(x)\rangle\langle j_\perp(0)\rangle, \quad (12)$$

where we have subtracted the finite local expectations (as one would do with density correlations). The main result of Ref. 11 was the absence of algebraic transverse current correlations in a C1S0 phase because of the strong spin fluctuations associated with the spin gap. Here, although the spin-gapped C1S0 phase survives at low flux, the situation is quite different because the chain exchange symmetry is explicitly broken by the magnetic field (Fig. 9). Indeed, Eq. (11) can be rewritten in the basis of the d,u bands, which leads in the continuum limit to terms with different wave vectors:

$$\begin{aligned} j_\perp(x) = it_\perp[&(a_u^2 - b_u^2)[e^{-2ik_u x}\psi_{u,R,\sigma}^\dagger\psi_{u,L,\sigma} - e^{2ik_u x}\psi_{u,u,\sigma}^\dagger\psi_{u,R,\sigma}] \\ &+ (a_d^2 - b_d^2)[e^{-2ik_d x}\psi_{d,R,\sigma}^\dagger\psi_{d,L,\sigma} - e^{2ik_d x}\psi_{d,L,\sigma}^\dagger\psi_{d,R,\sigma}] \\ &+ (b_u a_d + a_u b_d)[e^{-i(k_d+k_u)x}(\psi_{u,R,\sigma}^\dagger\psi_{d,L,\sigma} - \psi_{d,R,\sigma}^\dagger\psi_{u,L,\sigma}) \\ &+ e^{i(k_d+k_u)x}(\psi_{u,L,\sigma}^\dagger\psi_{d,R,\sigma} - \psi_{L,d,\sigma}^\dagger\psi_{u,R,\sigma})] + (b_u b_d + a_u a_d) \\ &\times[e^{-i(k_u-k_d)x}(\psi_{u,R,\sigma}^\dagger\psi_{d,R,\sigma} - \psi_{d,L,\sigma}^\dagger\psi_{u,L,\sigma}) \\ &+ e^{i(k_u-k_d)x}(\psi_{u,L,\sigma}^\dagger\psi_{d,L,\sigma} - \psi_{d,R,\sigma}^\dagger\psi_{u,R,\sigma})]], \end{aligned} \quad (13)$$

where the coefficients $a_{d/u}$ and $b_{d/u}$ are defined in Appendix C. We now turn to the bosonization representation of the operators appearing in Eq. (13). Terms with the lowest wave vector k_d-k_u contain operators of the form

$$\psi_{u,R,\sigma}^\dagger\psi_{d,R,\sigma} \sim e^{i[-\phi_{c-}+\theta_{c-}-\sigma(\phi_{s-}-\theta_{s-})]}, \quad (14)$$

with $\sigma=(\uparrow,\downarrow)=\pm$. In the C1S0 phase, their correlation functions decay exponentially as they involve the dual fields θ_{s-} and ϕ_{c-}, which are disordered. For the terms with the wave vector k_d+k_u, we find similarly that

$$\psi_{u,R,\sigma}^\dagger\psi_{d,L,\sigma} \sim e^{i[\phi_{c+}+\theta_{c-}+\sigma(\phi_{s+}+\theta_{s-})]}, \quad (15)$$

which also have short-ranged correlation functions because of the presence of the disordered field θ_{s-} in the bosonized representation Eq. (15). This is exactly the same result as in Ref. 11 albeit extended to nonzero flux. Without a magnetic field, DMRG calculations[11] showed that the dominant wave vector in the exponential signal was k^0+k^π rather than k^0-k^π, probably because the bosonized expression of the cor-

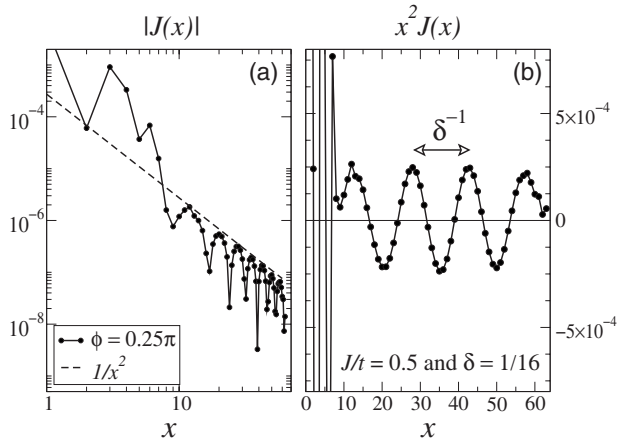

FIG. 9. (a) Transverse current correlations become algebraic in the C1S0 phase once the magnetic field is turned on (same parameters as in Fig. 8). (b) Demodulation of the signal enables to extract clearly the wave vector $2\pi\delta$ of the correlations.

responding Fourier component contains two strongly fluctuating fields for the latter term [see Eq. (14)], but only one [see Eq. (15)] for the former term. In the presence of a magnetic field, we see that the terms in Eq. (13) corresponding to the wave vectors $2k_u$ and $2k_d$ have a magnitude

$$(b_p)^2 - (a_p)^2 \propto \phi$$

at small flux ϕ, i.e., they exactly cancel for $\phi=0$, but are present once the magnetic field is turned on. These new terms are allowed by the symmetry reduction induced by the magnetic field. Furthermore, they have the bosonized expression:

$$\psi^\dagger_{p,R,\sigma}\psi_{p,L,\sigma} \sim e^{i[\phi_{c+}+p\phi_{c-}+\sigma(\phi_{s+}+p\phi_{s-})]}, \tag{16}$$

in which the spin contribution has long-range order, but the charge contribution contains the dual field ϕ_{c-}, leading to exponential decay of the associated correlation function. Therefore, all the $2k_F$ contributions in the transverse current correlation functions display and exponential decay.

In expression (13), the higher $4k_F$ harmonics of the current are not taken into account. The reason for this is that in the full Hillbert space, the $4k_F$ component of $j_\perp$ is simply proportional to $c^\dagger_{3k_F}c_{-k_F}$. However, in bosonization, a momentum cutoff is introduced, and the high-energy states which involve the creation or annihilation of fermions with momentum farther from the Fermi momenta than the cutoff are eliminated. Thus, the expression of the current at lowest order in the interaction U/t in Eq. (13) cannot contain any $4k_F$ contributions. However, virtual processes in which a fermion is created and annihilated far from the Fermi points give contributions of higher order in U/t to the $4k_F$ components that only involve fermion operators close to the Fermi points. Such contributions can be derived in perturbation theory following the approach in Refs. 42 and 43. In the case of the transverse current, an interaction of the form $Uc^\dagger_{k_F}c^\dagger_{k_F}c_{-k_F}c_{3k_F}$ yields a perturbative contribution proportional to $U/tc^\dagger_{k_F}c^\dagger_{k_F}c_{-k_F}c_{-k_F}$ to the $4k_F$ component, which involve only operators belonging to the low-energy subspace and, thus, cannot be neglected. Such corrections can be viewed as a pair hopping or a correlated hopping between the chains. Thus, we expect to find a $4k_F$ contribution to the transverse current of the form

$$\psi^\dagger_{d,R,\sigma}\psi_{d,L,\sigma}\psi^\dagger_{u,R,\sigma}\psi_{u,L,\sigma} \sim e^{i2\phi_{c+}}, \tag{17}$$

associated with the wave vector $2(k^d+k^u)=2\pi(1-\delta)$. The $\langle j_{\perp,4k_F}(x)j_{\perp,4k_F}(0)\rangle$ correlations have a power-law decay with exponent $2K_{c+}$. This result is very similar to the CDW fluctuations associated with the correlations $\langle n(x)n(0)\rangle$, which, while being short range at $2k_F$, also possess a $4k_F$ power-law decay.[6] Note that these CDW correlations contain terms analogous to Eqs. (14)–(16), but with different prefactors. This is in good agreement with numerical results, for which we found algebraic correlations with wave vector $2\pi\delta$. The wavelength of the correlations is again associated with the length scale δ^{-1} of the local hole and transverse current patterns. We found numerically a larger Luttinger exponent from the current correlations $K_{c+}\sim 1$, while superconducting correlations rather give $K_{c+}\sim 0.6$ for the same parameters.

TABLE I. Summary of the bosonization result for operators in the low-field C1S0 phase (see Appendix C for notations). We have $2k_F=\pi n$. If not short range ("Exp." notation), we give the decay exponent of the associated correlations. Numerically, $\langle n(x)n(0)\rangle$ and $\langle j_\perp(x)j_\perp(0)\rangle$ are algebraic because they pick up the $4k_F$ terms.

	In the C1S0 phase	
Operator	Exponent	Wave vector
$S^z(x)$	Exp.	$2k_F$
$\Delta(x)$	$1/(2K_{c+})$	0
$n_{2k_F}(x)$	Exp.	$2k_F$
$n_{4k_F}(x)$	$2K_{c+}$	$4k_F$
$j_{\perp,2k_F}(x)$	Exp.	$2k_F$
$j_{\perp,4k_F}(x)$	$2K_{c+}$	$4k_F$

This difference, also found for charge correlations,[2] could be attributed to the need for virtual high-energy processes to create the $4k_F$ correlations, leading to somehow low and noisy signals. The behavior of the bosonized operators is summarized in Table I.

B. Zero-field susceptibility and the commensurate phases

Since only very small flux per plaquette ϕ can be achieved experimentally, we now focus on the $\phi\to 0$ limit of the orbital susceptibility $\chi_0\equiv\chi^{\rm orb}(0)$, which is calculated numerically from Eq. (5). For the noninteracting system, this quantity is finite and positive at half-filling, and then increases with doping (see Fig. 16 of Appendix A). Once interactions are turned on, this susceptibility is zero at half-filling because of the Mott insulating state (see Fig. 10 and Appendix D for a general discussion of the susceptibility). When doped, the system acquires a susceptibility roughly

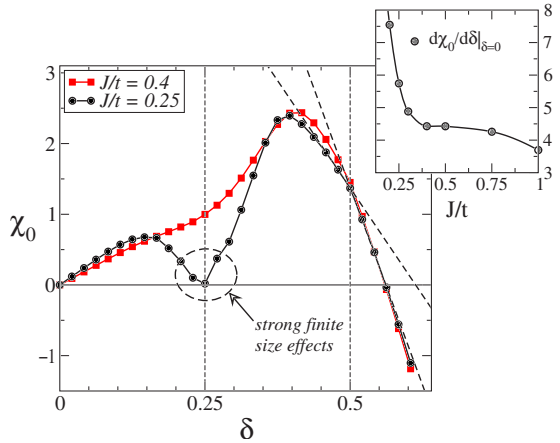

FIG. 10. (Color online) Zero-field susceptibility χ_0 as a function of doping δ and interaction parameters J/t for a ladder with $L=48$. A strong reduction at low J/t and commensurabilities $\delta=1/4$ and $1/2$ are clearly visible. The computed susceptibility is nearly zero at $\delta=1/4$, but subject to finite size effects (see Appendix B). On the contrary, the $\delta=1/2$ phase has a finite susceptibility. Inset: The derivative $d\chi_0/d\delta|_{\delta=0}$ as a function of J/t.

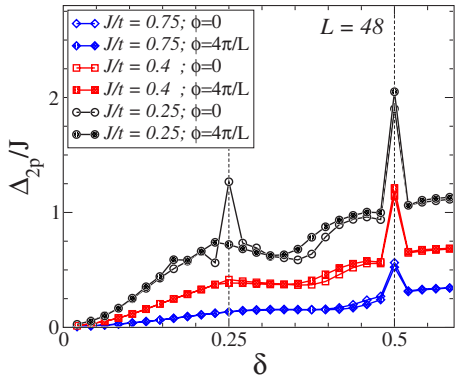

FIG. 11. (Color online) Two-particle charge gap as a function of doping showing the emergence of insulating phases at commensurabilities $\delta=1/2$ and $\delta=1/4$ at low J/t. The smallest flux we have access to is enough to destroy the $\delta=1/4$ CDW phase (see text for details), while the $\delta=0.5$ BOW phase is more stable. Data are computed with an extra $J=+0.3$ at the two extremal rungs.

proportional to the density of charge carriers with $\chi_0 \sim \delta$. The proportionality coefficient decreases with J/t, which is reminiscent of the fact that large J's reduce the mobility of holes (see inset of Fig. 10). Compared with the noninteracting result, the susceptibility is, thus, strongly reduced by the interaction. When the ratio J/t is lowered, a strong reduction of χ_0 is clearly visible for the hole commensurate doping $\delta=1/4$ up to finite size effects, as discussed in Appendix B. This drop of the susceptibility increases continuously as J/t is lowered (data not shown; for larger J/t, the convergence is better) so that we are confident that the observation is not an artifact of the finite size effects. For $\delta=1/2$, a discontinuity of the slope is found, but the susceptibility remains finite in this phase (there, the finite size effects are smaller). The occurrence of insulating CDWs was previously studied[6] in this part of the $(\delta, J/t)$ phase diagram of the t-J model. However, only the $\delta=1/4$ CDW phase was discussed and Fig. 10 suggests that the $\delta=1/2$ phase is of a different nature.

To study more precisely the occurrence of these phases, we have computed the two-particle charge gap

$$\Delta_{2p} = E_0(n_h+2) + E_0(n_h-2) - 2E_0(n_h) \tag{18}$$

as a function of doping and interaction at zero magnetic field and for the lowest flux $4\pi/L$ we have access to. A system with pairs always has a finite one-particle charge gap (or pairing energy), but is insulating if the two-particle charge gap is also finite. The results on a ladder of finite length $L=48$ are given in Fig. 11. On the one hand, a strong discontinuity at $\delta=1/2$ is found even for a rather large J/t, and the charge gap of this phase survives to nonzero flux (away from the commensurability, Δ_{2p} is much smaller but finite because of the finite length of the system). On the other hand, the $\delta=1/4$ discontinuity is only found at small J/t and is destroyed for the lowest flux we can use. No other discontinuity of the two-particle charge gap is found for the range of doping $0 \leqslant \delta \leqslant 0.6$. The system with $\delta=1/4$ has edge effects, and we have added an extra $J_\perp=+0.3$ on the two extremal rungs to control the spinons at the edges as was done in Ref. 6. This phase is, thus, difficult to study under a magnetic flux, but it was studied previously and it was proposed to be a fourfold degenerate CDW phase with pairing and a small spin gap on the basis of the behavior of the Friedel oscillations. These gaps were found to be numerically very small.[6] The observed sensitivity to the flux is consistent with small gaps. Indeed, such a fourfold degenerate phase is difficult to stabilize. Qualitatively, if pairs of holes are well formed on rungs, it is hard to generate an effective long-range repulsion between these pairs to stabilize a crystal of hole pairs. On the contrary, if pairs are spread over a few rungs, they can repel each other more easily, but will have a smaller spin gap and pairing energy. This latest picture of a pair of holes delocalized on a plaquette every two plaquettes seems to be more suited to describe this phase.

In the insulating phase with $\delta=1/2$ (quarter-filling), instead of the pronounced Friedel oscillations obtained for $\delta=1/4$, a uniform electronic density (see Fig. 12) is found. However, if one computes the bond order parameters $t_\nu(x)$ along the bonds at zero magnetic field by using the definitions

$$t_{1,\parallel}(x) = t_\parallel \langle c^\dagger_{x+1,1,\sigma} c_{x,1,\sigma} + c^\dagger_{x,1,\sigma} c_{x+1,1,\sigma} \rangle,$$

$$t_{2,\parallel}(x) = t_\parallel \langle c^\dagger_{x+1,2,\sigma} c_{x,2,\sigma} + c^\dagger_{x,2,\sigma} c_{x+1,2,\sigma} \rangle,$$

$$t_\perp(x) = t_\perp \langle c^\dagger_{x,1,\sigma} c_{x,2,\sigma} + c^\dagger_{x,2,\sigma} c_{x,1,\sigma} \rangle,$$

one finds strong oscillations with a period of two lattice sites for the $\parallel$ bonds, making this phase an insulating bond order wave (BOW) phase (see Fig. 13). This is confirmed by the current pattern under a magnetic field found in Fig. 12, which has well-defined orbits around plaquettes, but small currents between plaquettes. The local transverse current is staggered, while the transverse bond-density-wave order parameter is uniform. Such local orbits allow a finite orbital susceptibility even if the system remains insulating because $\langle j_\perp(x) j_\perp(0) \rangle \simeq \langle j_\perp(1) j_\perp(0) \rangle$ in Eq. (D2) which is simply the local response on a plaquette.

IV. CONCLUSION

We have studied the effect of a magnetic flux through a doped two-leg ladder by means of bosonization and DMRG

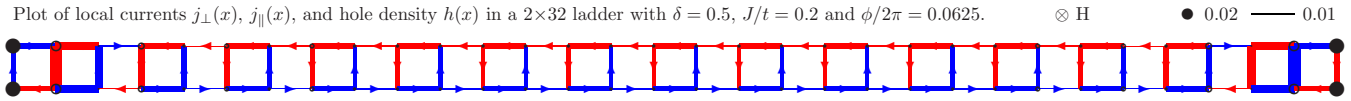

FIG. 12. (Color online) Local expectation values with the conventions of Fig. 8 on the $n=\delta=1/2$ line (quarter-filling) in the bond-density-wave phase at low flux.

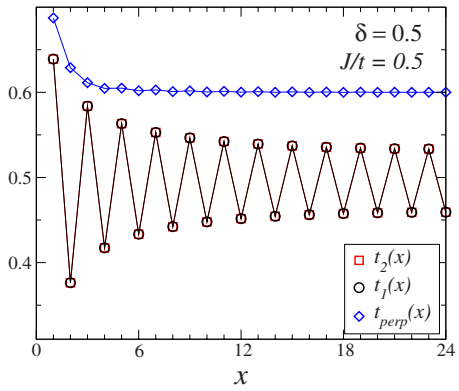

FIG. 13. (Color online) Local kinetic bonds $t_\nu(x)$ in the $\delta=1/2$ BOW phase computed at zero magnetic field. The parallel bond orders are strongly oscillating at wave vector π, while the transverse bond and the transverse kinetic bond and electronic densities are uniform (see Fig. 12).

calculations. As a function of the flux, a rich phase diagram is observed with an intermediate Luttinger liquid phase and the reentrance of the Luther-Emery phase at high flux. Both in the weak- and strong-coupling limits, the phase diagram is governed by the evolution of the band structure. Focusing on the small field physics of the Luther-Emery phase, we observe that local currents develop in the ladder inside the hole pair regions. Their typical length scale δ^{-1} is controlled by hole doping δ. The transverse current correlations also develop as soon as the magnetic field is turned on, with an algebraic behavior contrary to what was found without a magnetic field. Lastly, we have computed numerically the zero-field susceptibility of the system as a function of the interaction parameter J/t and of hole doping. We found that insulating commensurate phases at low J/t exist only at dopings $\delta=1/4$ and $1/2$, and that the two phases have different responses under a magnetic field. The contribution of the conduction electrons to the orbital susceptibility might, thus, be useful to probe these phases experimentally. Results on the $\delta=1/4$ phase are consistent with a fourfold degenerate ground state with a small pairing and spin gap, making it very sensitive to the flux. On the contrary, the $\delta=1/2$ phase appears to be a robust bond order wave phase with a twofold degenerate ground state. Despite its insulating nature, this phase has a finite susceptibility due to local orbits of electrons around plaquettes.

The ladder compound $Sr_{14-x}Ca_xCu_{24}O_{41}$ (SCCO) was the first nonsquare cuprate compound showing superconductivity under high pressure.[44] The presence of a spin gap in its superconducting phase has been addressed experimentally,[45–48] but no consensus has risen on the actual nature of superconductivity in this material. Another exciting feature of SCCO is the occurrence of charge density waves at ambient pressure.[49–58] Experiments[57,58] have suggested that CDW could appear at wave vectors $1/3$ and $1/5$, which was discussed theoretically using a multiband charge transfer model solved by Hartree-Fock approximation.[59] Here, we have shown that the t-J model on a single ladder only displays $1/4$ and $1/2$ commensurabilities, as proposed in Ref. 6, and that orbital susceptibility could help to understand the nature of these commensurate phases.

We would like to point out that an interesting realization of quasi-one-dimensional systems in which magnetic flux can affect the band structure is provided by carbon nanotubes.[60] Following the theoretical prediction,[60] experiments on multiwall nanotubes (where notable fluxes can be achieved due to the large diameter of the outmost shell) have shown that the band structure of these systems was indeed sensitive to magnetic fluxes.[61–63] In the case of gapped zigzag single wall nanotubes, although the experimentally accessible fluxes through the tubes were small, an effect on the conductance oscillations in the Fabry-Perot regime could, nevertheless, be evidenced as a result of the lifting of the degeneracy between two subbands. As there exists some evidence for strong electronic correlations in carbon nanotubes,[64–68] and as carbon nanotubes possess some analogies with ladders,[69] an interesting extension of the theoretical results developed in the present paper would be to study quasi-one-dimensional models mimicking more closely carbon nanotubes. It would be particularly interesting to compute the behavior of the Luttinger exponent controlling the zero bias anomaly as a function of the applied field.

ACKNOWLEDGMENTS

G.R. would like to thank IDRIS (Orsay, France) and CALMIP (Toulouse, France) for use of supercomputer facilities. G.R. and D.P. thank Agence Nationale de la Recherche (France) for support. G.R. and S.R.W. acknowledge the support of the NSF under Grant No. DMR-0605444.

APPENDIX A: FORMULAS FOR THE NONINTERACTING SYSTEM

Part of these results was first given in Refs. 22 and 23. We reproduce them for clarity and notation conventions (which are different) and extend them when necessary. In what follows, $\alpha=t_\perp/t_\parallel$.

1. Band structure

At zero flux, the interchain coupling lifts the degeneracy between chains, giving birth to a bonding band $k_y=0$ and an antibonding band $k_y=\pi$. The flux breaks the reflection symmetry between chains, and couples these 0 and π modes. We call down and up (with labels d/u) the two bands in the presence of a flux. It is straightforward to diagonalize the noninteracting Hamiltonian by taking the Fourier transform, which gives the energies

$$\mathcal{E}_{d/u}(k,\phi) = -2t_\parallel\left\{\cos k\cos\frac{\phi}{2} \pm \sqrt{\sin^2 k\sin^2\frac{\phi}{2}+\left(\frac{\alpha}{2}\right)^2}\right\}. \tag{A1}$$

The basis transformation can be written using coherence factors $a_k, b_k > 0$

$$\begin{pmatrix} c_{k,1} \\ c_{k,2} \end{pmatrix} = \begin{pmatrix} a_k & b_k \\ b_k & -a_k \end{pmatrix}\begin{pmatrix} c_{k,d} \\ c_{k,u} \end{pmatrix}, \tag{A2}$$

with

$$a_k^2 = \frac{1}{2}\left(1 - \frac{\sin k \sin\frac{\phi}{2}}{\sqrt{\sin^2 k \sin^2\frac{\phi}{2} + \left(\frac{\alpha}{2}\right)^2}}\right), \tag{A3}$$

$$b_k^2 = \frac{1}{2}\left(1 + \frac{\sin k \sin\frac{\phi}{2}}{\sqrt{\sin^2 k \sin^2\frac{\phi}{2} + \left(\frac{\alpha}{2}\right)^2}}\right). \tag{A4}$$

We have $a_{-k}=b_k$, and the factors depend on the wave vector k, while at zero flux, $a_k=b_k=1/\sqrt{2}$. For any finite flux and $k>0$, we have $a_k<b_k$ with

$$b_k^2 - a_k^2 = \frac{\sin k \sin\frac{\phi}{2}}{\sqrt{\sin^2 k \sin^2\frac{\phi}{2} + \left(\frac{\alpha}{2}\right)^2}}. \tag{A5}$$

Below are a few considerations on the band structure (A1), which are summarized in Fig. 2:

(i) The condition to have a band gap is that $\max \mathcal{E}_d = \mathcal{E}_d(\pi,\phi) < \min \mathcal{E}_u = \mathcal{E}_u(0,\phi)$, which gives $\frac{\alpha}{2}=\cos\frac{\phi}{2}$. This condition can be reformulated as $\phi>\phi_0$ with

$$\sin\frac{\phi_0}{2} = \sqrt{1-\left(\frac{\alpha}{2}\right)^2}. \tag{A6}$$

(ii) The condition to have a double well in the $\mathcal{E}_d$ band comes from the sign of the second derivative at $k=0$ and is $\frac{\alpha}{2}\cos\frac{\phi}{2}=\sin^2\frac{\phi}{2}$. This condition can be reformulated as $\phi>\phi_c$ with

$$\sin\frac{\phi_c}{2} = \left[\frac{\sqrt{\alpha^4+16\alpha^2}-\alpha^2}{8}\right]^{1/2}. \tag{A7}$$

In this case, the wave vectors corresponding to the minimum of the down band and the maximum of the up band read

$$k^d_{\min}(\phi) = \arcsin\sqrt{\sin^2\frac{\phi}{2} - \left(\frac{\alpha}{2}\right)^2\cot^2\frac{\phi}{2}}, \tag{A8}$$

$$k^u_{\max}(\phi) = \pi - k^d_{\min}(\phi), \tag{A9}$$

which appears with a finite value.

(iii) The two curves' intersection is $\alpha=\sqrt{2}$, for which we have $\phi_{0/c}=\pi/2$. If $\alpha<\alpha_c$, we have $\phi_c<\phi_0$; else, $\phi_0<\phi_c$.

(iv) The condition to empty the u band is $\mu=\alpha-2\cos\frac{\phi}{2}$, and is the same as the condition for which the d band is completely filled.

(v) We can show that only situations with two or four Fermi points can occur: for monotonous bands ($\phi<\phi_c$), this is obvious. For nonmonotonous dispersion ($\phi>\phi_c$), if $\phi>\phi_0$, the two bands are not overlapping so we have either two or four Fermi points. For any flux $\phi\in[\phi_c,\phi_0]$, we can convince ourselves that since $\mathcal{E}^u(k,\phi)>\mathcal{E}^d(k,\phi)$ (for any k) and since the up band has a unique maximum [at $k^u_{\max}(\phi)$], while the down band has a unique minimum [at $k^d_{\min}(\phi)$], it necessarily implies that only two or four Fermi points are allowed (see Fig. 14).

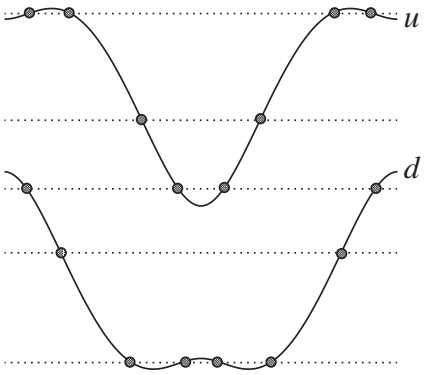

FIG. 14. Depending on the filling, the number of Fermi points can be either 2 or 4 (sketched on the bands of the B phase of Fig. 2). Note that at low and high fillings, the two Fermi velocities have opposite signs, while at intermediate filling, they have the same sign.

2. Filling the bands: Finding Fermi points

Fermi points $k_F^{d/u}$ are deduced from their relation to the chemical potential μ from Eq. (A1). If needed, this equation can be inverted into

$$\cos k_F^{d/u}(\mu,\phi) = -\frac{\mu}{2t_\parallel}\cos\frac{\phi}{2} \pm s_{d/u}\sqrt{\left[1-\left(\frac{\mu}{2t_\parallel}\right)^2\right]\sin^2\frac{\phi}{2}+\left(\frac{\alpha}{2}\right)^2}. \tag{A10}$$

This previous expression is useful when working at fixed μ. Note that, depending on ϕ and μ, the above equation can have two roots labeled by $s_{d/u}=\pm 1$ for *each* sector d and u (see Fig. 14). If there are two Fermi points in the same band p, we use the notation $k^p_{F,1/2}$. The Fermi velocities can be evaluated from

$$v_F^{d/u}(k,\phi) = 2t_\parallel \sin k\left\{\cos\frac{\phi}{2} \mp \frac{\cos k \sin^2\frac{\phi}{2}}{\sqrt{\sin^2 k \sin^2\frac{\phi}{2}+\left(\frac{\alpha}{2}\right)^2}}\right\}. \tag{A11}$$

Note that one of the two Fermi velocities is negative in the case of nonmonotonous bands.

Working at fixed electronic density n, we have to relate the Fermi points directly to n using Eq. (A1) and the Luttinger sum rule (see Fig. 14 for a sketch of all possible situations). If the system has only two Fermi points, then we have either $k_F^d=\pi n$ or $k_F^u=\pi(n-1)$, where both relations do not depend on the flux. When there are four Fermi points and limiting the discussion to $n\leqslant 1$, we have either that

(i) the bands are overlapping:

$$k_F^u + k_F^d = \pi n,$$

$$\sin\left(\frac{k_F^u - k_F^d}{2}\right) = \left[\frac{\left(\frac{\alpha}{2}\right)^2 \cos^2\frac{\phi}{2}}{\sin^2\left(\frac{\pi n}{2}\right) - \sin^2\frac{\phi}{2}} + \sin^2\frac{\phi}{2}\right]^{1/2};$$

(ii) there is a nonmonotonous dispersion, for the down band:

$$k_{F,1}^d - k_{F,2}^d = \pi n,$$

$$\sin\left(\frac{k_{F,1}^d + k_{F,2}^d}{2}\right) = \left[\frac{\left(\frac{\alpha}{2}\right)^2 \cos^2\frac{\phi}{2}}{\sin^2\left(\frac{\pi n}{2}\right) - \sin^2\frac{\phi}{2}} + \sin^2\frac{\phi}{2}\right]^{1/2}.$$

These equations reproduce the correct result in the $\phi=0$ and $\alpha=0$ limits. It is also straightforward to compute the four critical densities at which the number of Fermi points changes from two to four and from four to two (see Fig. 3). By arranging them according to $n_{c1}<n_{c2}<n_{c3}<n_{c4}$, we have

$$n_{c1} = \arccos[\cos\phi + \alpha\cos(\phi/2)]/\pi \quad \text{if } \phi \in [\phi_c, \pi],$$

$$n_{c2} = \arccos[\cos\phi - \alpha\cos(\phi/2)]/\pi \quad \text{if } \phi \in [0, \phi_0],$$

$$n_{c3} = 2 - n_{c2} \quad \text{if } \phi \in [0, \phi_0],$$

$$n_{c4} = 2 - n_{c1} \quad \text{if } \phi \in [\phi_c, \pi]. \tag{A12}$$

These equations can be inverted to give the critical flux $\phi^{2\leftrightarrow 4}$ at which the transitions from $2\leftrightarrow 4$ Fermi points occur:

$$\cos\frac{\phi^{2\leftrightarrow 4}}{2} = \frac{1}{2}\left[\pm\frac{\alpha}{2} + \sqrt{\left(\frac{\alpha}{2}\right)^2 + 4\cos^2\left(\frac{\pi n}{2}\right)}\right]. \tag{A13}$$

This last expression is useful for checking that the change of sign of the susceptibility is associated with these transitions.

3. Orbital susceptibility

Knowing the location of the Fermi points, we can compute quantities integrated over the bands such as the total energy $E_0(\phi)$, the screening current $j_\parallel(\phi)$, and the associated orbital susceptibility from Eqs. (5). One contribution to this current from electrons of momentum k is $j_\parallel^{d/u}(k,\phi) = \partial\mathcal{E}_{d/u}(k,\phi)/\partial\phi$, which reads

$$j_\parallel^{d/u}(k,\phi) = -t_\parallel\left\{\cos k \sin\frac{\phi}{2} \mp \frac{1}{2}\frac{\sin^2 k \sin\phi}{\sqrt{\sin^2 k \sin^2\frac{\phi}{2} + \left(\frac{\alpha}{2}\right)^2}}\right\}, \tag{A14}$$

and similarly, the corresponding contribution to the susceptibility reads

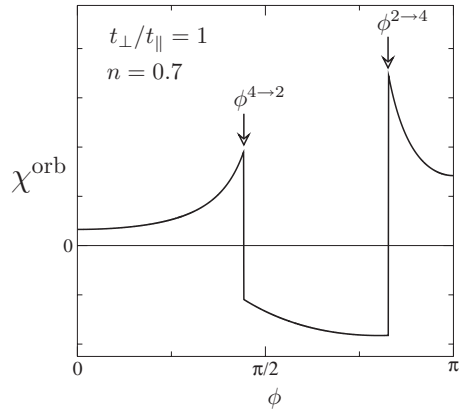

FIG. 15. Susceptibility as a probe to the number of Fermi points for $0.5<1-\delta<1.0$ and $t_\perp=t_\parallel$. $\phi^{2\leftrightarrow 4}$ indicates the transitions from four to two and from two to four Fermi points.

$$\chi_{d/u}^{\rm orb}(k,\phi) = -\frac{t_\parallel}{2}\left\{\cos k\cos\frac{\phi}{2} \mp \frac{\sin^2 k\cos\phi}{\left[\sin^2 k\sin^2\frac{\phi}{2} + \left(\frac{\alpha}{2}\right)^2\right]^{1/2}} \pm \frac{1}{4}\frac{\sin^4 k\sin^2\phi}{\left[\sin^2 k\sin^2\frac{\phi}{2} + \left(\frac{\alpha}{2}\right)^2\right]^{3/2}}\right\}. \tag{A15}$$

It is important to remark that additional contributions come from the derivatives $\partial k^p(\phi)/\partial\phi$ and $\partial^2 k^p(\phi)/\partial\phi^2$ because, in the case of four Fermi points, the location of the Fermi points depends on the flux. Thus, Eqs. (5) can be computed either analytically or numerically. A typical plot of the integrated $\chi^{\rm orb}(\phi)$ is given in Fig. 15, which shows that its discontinuities are associated with the $2\leftrightarrow 4$ Fermi point transitions of Eqs. (A13). We have checked that the latest result is valid only for $0.5<n=1-\delta<1.0$ when $\alpha=1$ (see zero-field susceptibility below).

Lastly, the behavior of the zero-field susceptibility $\chi_0^{\rm orb}$ can be computed as a function of the electronic density n. With a factor 2 for the spins, we have the following:

if $\alpha>1-\cos\pi n$ (two Fermi points),

$$\chi_0^{\rm orb}(n) = -t_\parallel\left[\sin\pi n\left(1 + \frac{1}{\alpha}\cos\pi n\right) - \frac{\pi}{\alpha}n\right]; \tag{A16}$$

else, if $\alpha<1-\cos\pi n$ (four Fermi points), we have

$$\chi_0^{\rm orb}(n) = -t_\parallel\left[\sqrt{\sin^2\left(\frac{\pi n}{2}\right) - \left(\frac{\alpha}{2}\right)^2}\left(2 + \frac{\cos\pi n}{\sin^2(\pi n/2)}\right) - \frac{2}{\alpha}\arcsin\left(\frac{\alpha}{2}\frac{1}{\sin(\pi n/2)}\right)\right]. \tag{A17}$$

The curve for $\alpha=1$ is plotted in Fig. 16, which shows that for $n<0.5$, even when there are only two Fermi points, the susceptibility can be either positive or negative.

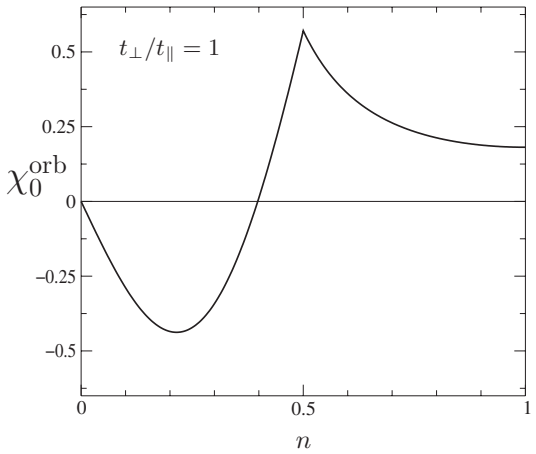

FIG. 16. Zero-field orbital susceptibility of the noninteracting system for $t_\perp = t_\parallel$ from Eqs. (A16) and (A17). The singularity at $n=0.5$ marks the transition from two to four Fermi points. When $n<0.5$, the susceptibility changes sign for $n \simeq 0.3975\ldots$, while the system always has two Fermi points.

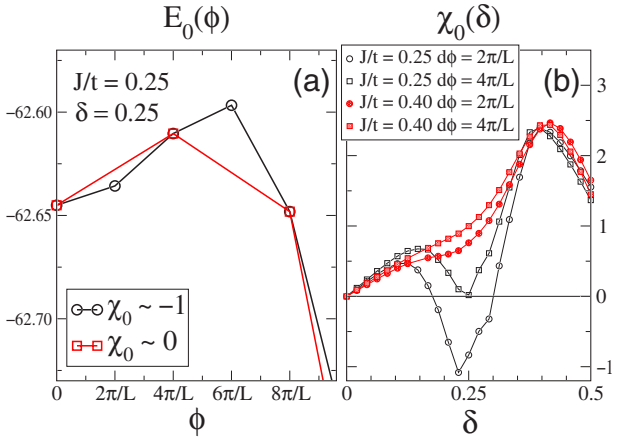

FIG. 17. (Color online) Finite size effects on the calculation of the zero-field susceptibility at low J/t. (a) energies as a function of flux. (b) χ_0 as a function of the doping δ from Eq. (B2) for two different $d\phi$.

APPENDIX B: FLUX QUANTIZATION AND FINITE SIZE EFFECTS

In this section, we discuss the quantization of the flux on a finite size ladder. First, Hamiltonian (1) clearly gives $E(\phi)=E(2\pi-\phi)$ so that we can restrict ourselves to the window $\phi \in [0,\pi]$. Similarly, from Eqs. (5), we have $j(\phi)=-j(2\pi-\phi)$, which implies that $j(0)=j(\pi)=0$. What is quantization of the flux ϕ on a finite system? By using periodic boundary conditions with the gauge of Fig. 1, the integrated flux along a leg is $\pm(\phi/2)L$ so that there is no remanent flux through the *cylinder hole* of the periodic ladder if

$$\phi = m4\pi/L, \tag{B1}$$

with m an integer. Actually, this can also be simply understood from momentum quantization $k=2\pi m/L$ and by looking at the dispersions $-2t_\parallel \cos(k \pm \phi/2)$ on each leg when $t_\perp=0$. This quantization can be checked numerically with exact diagonalization. Furthermore, another possible gauge which gives the same flux per plaquette is to take $\phi_\perp(x)=\phi x$, with $\phi_\perp$ the flux along a rung, and no flux along the legs. We can show that the two gauges are strictly equivalent on a finite system with periodic boundary conditions only if Eq. (B1) is satisfied.

With DMRG, we are using open boundary conditions for which we expect similar effects due to momentum quantization. For most quantities and parameters J/t, the points with $\phi=2\pi m/L$ interpolate nicely with the ones using Eq. (B1) so we can relax the constraint (see Fig. 4, for instance). However, when taking the derivatives such as in Eq. (5) at low J/t where more finite size effects are present, one must strictly obey Eq. (B1) to have correct estimates (this is necessary in Fig. 10, for instance). In Fig. 17, because we know that $j_\parallel(0)=0$, the zero-field susceptibility is

$$\chi_0 = [E_0(2d\phi) - E_0(0)]/2d\phi^2. \tag{B2}$$

Taking $d\phi=2\pi/L$ gives a negative susceptibility, while $d\phi=4\pi/L$ gives $\chi_0 \sim 0$. Finite size effects are smaller away from the $\delta=0.25$ commensurability and also at larger J/t.

The DMRG simulations were performed using the standard finite system algorithm on systems ranging from $L=32$ to $L=64$, with minor modifications to treat complex wave functions. The density matrix at each step was the sum of the density matrices constructed using the real and imaginary parts separately. Typically, we kept $m=1400$ states per block, giving a typical truncation error of 10^{-6}. The presence of the magnetic field did not increase the truncation error notably. Correlation functions are computed by averaging two-point correlations of equal distance. Correlations with one point too close to one of the edges are removed. Even if there is no translation symmetry with open boundary conditions, this method gives comparable results with the one using one point fixed at the middle (but this method gives access to a larger distance x).

APPENDIX C: BOSONIZATION CONVENTIONS

We use the same conventions as in Ref. 70. The bosonization procedure starts from the linearization of the band dispersion in the vicinity of the Fermi points. When there are four Fermi points, two of them in the up band and the two other in the down band (corresponding to the low-field C1S0 phase), we use

$$\begin{pmatrix} c_1 \\ c_2 \end{pmatrix} = \frac{1}{\sqrt{L}} \sum_k e^{ikx} \begin{pmatrix} a_k & b_k \\ b_k & -a_k \end{pmatrix} \begin{pmatrix} c_{k,d} \\ c_{k,u} \end{pmatrix},$$

with implicit spin index if not explicitly required. We denote by $\psi_{R/L,d/u}$ the bosonized right and left movers inside each band. Note that we have different Fermi levels $k_{F,d} \equiv k_d \neq k_{F,u} \equiv k_u$. From Eqs. (A3) and (A4), we deduce that $a_{-k_{d/u}} = b_{k_{d/u}} \equiv b_{d/u}$ and $b_{-k_{d/u}} = a_{k_{d/u}} \equiv a_{d/u}$. The bosonized version of the local fermion operators depends on how many Fermi

points we have and which bands are filled. If we have four Fermi points and overlapping bands, we use

$$c_1(x)/\sqrt{a} \to a_d e^{ik_d x}\psi_{d,R}(x) + b_d e^{-ik_d x}\psi_{d,L}(x) + b_u e^{ik_u x}\psi_{u,R}(x) + a_u e^{-ik_u x}\psi_{u,L}(x),$$

$$c_2(x)/\sqrt{a} \to b_d e^{ik_d x}\psi_{d,R}(x) + a_d e^{-ik_d x}\psi_{d,L}(x) - a_u e^{ik_u x}\psi_{u,R}(x) - b_u e^{-ik_u x}\psi_{u,L}(x),$$

where the right and left moving Fermi fields have the bosonized representation

$$\psi_{p,r,\sigma} = \frac{\eta^r_{p,\sigma}}{\sqrt{2\pi\alpha}} e^{i\epsilon_r \phi_{r,p,\sigma}},$$

with α a cutoff (not $t_\perp/t_\parallel$), $r=R/L$, $p=d/u$, and $\epsilon_{R/L}=\mp 1$. $\eta^r_{p,\sigma}$ are Klein factors that ensure anticommutation of fermion operators having different spins or band indices. The fields $\phi_{r,p,\sigma}$ are chiral boson fields. The nonchiral bosons fields are defined by

$$\phi_{p,\sigma} = [\phi_{L,p,\sigma} + \phi_{R,p,\sigma}]/2, \tag{C1}$$

$$\theta_{p,\sigma} = [\phi_{L,p,\sigma} - \phi_{R,p,\sigma}]/2, \tag{C2}$$

and they satisfy commutation relations $[\phi_{p,\sigma}(x), \theta_{p',\sigma'}(x')] = i\delta_{pp'}\delta_{\sigma,\sigma'}\delta(x-x')$. As usual in the framework of two coupled chains, we also introduce the following combinations of the ϕ and θ fields: the charge and spin modes in each bands p are

$$\phi_{c,p} = [\phi_{p,\uparrow} + \phi_{p,\downarrow}]/\sqrt{2}, \tag{C3}$$

$$\phi_{s,p} = [\phi_{p,\uparrow} - \phi_{p,\downarrow}]/\sqrt{2}, \tag{C4}$$

and similar transformations for the θ. And lastly, the $\pm$ combinations

$$\phi_{c/s,\pm} = [\phi_{c/s,d} \pm \phi_{c/s,u}]/\sqrt{2}. \tag{C5}$$

The Luttinger parameters associated with these bosons are $K_{c\pm}$ for the charge sectors and $K_{s\pm}$ for the spin sectors.

In the case of two Fermi points (intermediate flux C1S1 phase) and $n<1$, only the down band is filled, and we can use the results of a single chain, but using

$$c_1(x)/\sqrt{a} \to a_d e^{ik_d x}\psi_{d,R}(x) + b_d e^{-ik_d x}\psi_{d,L}(x),$$

$$c_2(x)/\sqrt{a} \to b_d e^{ik_d x}\psi_{d,R}(x) + a_d e^{-ik_d x}\psi_{d,L}(x).$$

We simply denote by K_c and K_s the Luttinger parameters corresponding to the charge and spin modes, respectively.

In the high-flux C1S0 phase, four points are present in the down band. With the notation $k_{F,1,d} \equiv k_1 \neq k_{F,2,d} \equiv k_2$, we have, after linearizing the band structure,

$$c_1(x)/\sqrt{a} \to a_1 e^{ik_1 x}\psi_{1,R}(x) + b_1 e^{-ik_1 x}\psi_{1,L}(x) + a_2 e^{ik_2 x}\psi_{2,L}(x) + b_2 e^{-ik_2 x}\psi_{2,R}(x),$$

$$c_2(x)/\sqrt{a} \to b_1 e^{ik_1 x}\psi_{1,R}(x) + a_1 e^{-ik_1 x}\psi_{1,L}(x) + b_2 e^{ik_2 x}\psi_{2,L}(x) + a_2 e^{-ik_2 x}\psi_{2,R}(x),$$

and similar expressions for the Fermi operators $\psi_{p,r}(x)$.

APPENDIX D: DIAMAGNETIC SUSCEPTIBILITY

Let us consider the Hamiltonian (3) or (4) in the limit $\phi \to 0$. By expanding to second order, we have

$$\mathcal{H} = \mathcal{H}(\phi=0) - \frac{\phi}{2}L(j_1 - j_2) - \frac{\phi^2}{8}L(K_1 + K_2),$$

where $j_{1,2}$ are the densities of current operators along chains 1 and 2, and $K_{1,2}$ represent the densities of kinetic energy in chains 1 and 2. Note that these operators are taken at $\phi=0$. We obtain the density of screening current operator $j_\parallel = -\frac{1}{L}\partial\mathcal{H}/\partial\phi$ as

$$j_\parallel = \frac{1}{2}(j_1 - j_2) + \frac{\phi}{4}(K_1 + K_2).$$

Using linear response theory, we obtain the expectation value of this current in this limit as

$$j_\parallel(\phi) = \langle j_\parallel\rangle_0 = \frac{\phi}{4}[\langle\langle (j_1 - j_2); (j_1 - j_2)\rangle\rangle_0 + \langle K_1 + K_2\rangle_0],$$

where $\langle\langle ;\rangle\rangle_0$ represents the retarded response function and $\langle\ \rangle_0$ is the expectation value in the ground state without a magnetic field. In the absence of interchain hopping, the cross response function $\langle\langle j_1; j_2\rangle\rangle_0$ would vanish and $\langle j_\parallel\rangle_0$ would be simply the sum of Drude weights of each chain. The expression of $\langle j_\parallel\rangle_0$ can be rearranged by noting that

$$j_1 - j_2 = 2\int^x j_\perp \tag{D1}$$

as a consequence of Kirchhoff's law. So we have that

$$\chi_0 = \int dx \langle j_\perp(x) j_\perp(0)\rangle_0 + \frac{1}{4}\langle K_1 + K_2\rangle_0. \tag{D2}$$

In the case of negligible transverse current correlations, this term reduces to the expectation value of the kinetic energy. In an insulator, this yields a vanishing diamagnetic susceptibility.

*roux@irsamc.ups-tlse.fr

[1] E. Dagotto, J. Riera, and D. Scalapino, Phys. Rev. B **45**, 5744 (1992).
[2] C. A. Hayward, D. Poilblanc, R. M. Noack, D. J. Scalapino, and W. Hanke, Phys. Rev. Lett. **75**, 926 (1995).
[3] M. Troyer, H. Tsunetsugu, and T. M. Rice, Phys. Rev. B **53**, 251 (1996).
[4] L. Balents and M. P. A. Fisher, Phys. Rev. B **53**, 12133 (1996).
[5] H. J. Schulz, Phys. Rev. B **53**, R2959 (1996).
[6] S. R. White, I. Affleck, and D. J. Scalapino, Phys. Rev. B **65**, 165122 (2002).
[7] P. W. Anderson, Science **235**, 1196 (1987).
[8] N. Nagaosa, Solid State Commun. **94**, 495 (1995).
[9] S. T. Carr and A. M. Tsvelik, Phys. Rev. B **65**, 195121 (2002).
[10] A. A. Nersesyan, Phys. Lett. A **153**, 49 (1991).
[11] D. J. Scalapino, S. R. White, and I. Affleck, Phys. Rev. B **64**, 100506(R) (2001).
[12] K. Tsutsui, D. Poilblanc, and S. Capponi, Phys. Rev. B **65**, 020406(R) (2001).
[13] U. Schollwöck, S. Chakravarty, J. O. Fjærestad, J. B. Marston, and M. Troyer, Phys. Rev. Lett. **90**, 186401 (2003).
[14] J. O. Fjærestad, J. B. Marston, and U. Schollwöck, Ann. Phys. (N.Y.) **321**, 894 (2006).
[15] T. Kjeldaas and W. Kohn, Phys. Rev. **105**, 806 (1957).
[16] J. E. Hebborn and E. H. Sondheimer, Phys. Rev. Lett. **2**, 150 (1959).
[17] W. Kohn, Phys. Rev. **115**, 1460 (1959).
[18] D. C. Cabra, A. De Martino, P. Pujol, and P. Simon, Europhys. Lett. **57**, 402 (2002).
[19] G. Roux, S. R. White, S. Capponi, and D. Poilblanc, Phys. Rev. Lett. **97**, 087207 (2006).
[20] G. Roux, E. Orignac, P. Pujol, and D. Poilblanc, Phys. Rev. B **75**, 245119 (2007).
[21] A. F. Albuquerque and G. B. Martins, J. Phys.: Condens. Matter **17**, 2419 (2005).
[22] B. N. Narozhny, S. T. Carr, and A. A. Nersesyan, Phys. Rev. B **71**, 161101(R) (2005).
[23] S. T. Carr, B. N. Narozhny, and A. A. Nersesyan, Phys. Rev. B **73**, 195114 (2006).
[24] E. Orignac and T. Giamarchi, Phys. Rev. B **64**, 144515 (2001).
[25] S. R. White, Phys. Rev. Lett. **69**, 2863 (1992).
[26] S. R. White, Phys. Rev. B **48**, 10345 (1993).
[27] U. Schollwöck, Rev. Mod. Phys. **77**, 259 (2005).
[28] R. E. Peierls, Z. Phys. **80**, 763 (1933).
[29] W. Kohn, Phys. Rev. **133**, A171 (1964).
[30] P. Gagliardini, S. Haas, and T. M. Rice, Phys. Rev. B **58**, 9603 (1998).
[31] C. M. Varma and A. Zawadowski, Phys. Rev. B **32**, 7399 (1985).
[32] K. Penc and J. Sólyom, Phys. Rev. B **41**, 704 (1990).
[33] M. Fabrizio, Phys. Rev. B **48**, 15838 (1993).
[34] H. H. Lin, L. Balents, and M. P. A. Fisher, Phys. Rev. B **56**, 6569 (1997).
[35] M. Fabrizio, Phys. Rev. B **54**, 10054 (1996).
[36] S. Daul and R. M. Noack, Phys. Rev. B **58**, 2635 (1998).
[37] C. Bourbonnais and L. G. Caron, Physica B & C **143B**, 450 (1986).
[38] C. Bourbonnais and L. G. Caron, Int. J. Mod. Phys. B **5**, 1033 (1991).
[39] G. Roux, S. R. White, S. Capponi, A. Läuchli, and D. Poilblanc, Phys. Rev. B **72**, 014523 (2005).
[40] D. Poilblanc, O. Chiappa, J. Riera, S. R. White, and D. J. Scalapino, Phys. Rev. B **62**, R14633 (2000).
[41] D. Poilblanc, E. Orignac, S. R. White, and S. Capponi, Phys. Rev. B **69**, 220406(R) (2004).
[42] K. Penc and J. Sólyom, Phys. Rev. B **44**, 12690 (1991).
[43] M. Tsuchiizu, H. Yoshioka, and Y. Suzumura, J. Phys. Soc. Jpn. **70**, 1460 (2001).
[44] M. Uehara, T. Nagata, J. Akimitsu, H. Takahashi, N. Môri, and K. Kinoshita, J. Phys. Soc. Jpn. **65**, 2764 (1996).
[45] H. Mayaffre, P. Auban-Senzier, M. Nardone, D. Jérome, D. Poilblanc, C. Bourbonnais, U. Ammerahl, G. Dhalenne, and A. Revcolevschi, Science **279**, 345 (1998).
[46] D. Jérome, P. Auban-Sauzier, and Y. Piskunov, in *High Magnetic Fields*, edited by C. Berthier, L. P. Lévy, and G. Martinez, Lecture Notes in Physics Vol. 595 (Springer, New York, 2002).
[47] N. Fujiwara, N. Môri, Y. Uwatoko, T. Matsumoto, N. Motoyama, and S. Uchida, Phys. Rev. Lett. **90**, 137001 (2003).
[48] N. Fujiwara, N. Môri, Y. Uwatoko, T. Matsumoto, N. Motoyama, and S. Uchida, J. Phys.: Condens. Matter **17**, S929 (2005).
[49] T. Osafune, N. Motoyama, H. Eisaki, S. Uchida, and S. Tajima, Phys. Rev. Lett. **82**, 1313 (1999).
[50] B. Gorshunov, P. Haas, T. Rõõm, M. Dressel, T. Vuletić, B. Korin-Hamzić, S. Tomić, J. Akimitsu, and T. Nagata, Phys. Rev. B **66**, 060508(R) (2002).
[51] G. Blumberg, P. Littlewood, A. Gozar, B. S. Dennis, N. Motoyama, H. Eisaki, and S. Uchida, Science **297**, 584 (2002).
[52] T. Vuletić, B. Korin-Hamzić, S. Tomić, B. Gorshunov, P. Haas, T. Rõõm, M. Dressel, J. Akimitsu, T. Sasaki, and T. Nagata, Phys. Rev. Lett. **90**, 257002 (2003).
[53] P. Abbamonte, G. Blumberg, A. Rusydi, A. Gozar, P. G. Evans, T. Siegrist, L. Venema, H. Eisaki, E. D. Isaacs, and G. A. Sawatzky, Nature (London) **431**, 1078 (2004).
[54] A. Gozar and G. Blumberg, *Frontiers in Magnetic Materials* (Springer-Verlag, Berlin, 2005), p. 653.
[55] T. Vuletić, T. Ivek, B. Korin-Hamzić, S. Tomić, B. Gorshunov, P. Haas, M. Dressel, J. Akimitsu, T. Sasaki, and T. Nagata, Phys. Rev. B **71**, 012508 (2005).
[56] K.-Y. Choi, M. Grove, P. Lemmens, M. Fischer, G. Guntherodt, U. Ammerahl, B. Buchner, G. Dhalenne, A. Revcolevschi, and J. Akimitsu, Phys. Rev. B **73**, 104428 (2006).
[57] A. Rusydi, P. Abbamonte, H. Eisaki, Y. Fujimaki, G. Blumberg, S. Uchida, and G. A. Sawatzky, Phys. Rev. Lett. **97**, 016403 (2006).
[58] A. Rusydi, M. Berciu, P. Abbamonte, S. Smadici, H. Eisaki, Y. Fujimaki, S. Uchida, M. Rubhausen, and G. A. Sawatzky, Phys. Rev. B **75**, 104510 (2007).
[59] K. Wohlfeld, A. M. Oles, and G. A. Sawatzky, Phys. Rev. B **75**, 180501(R) (2007).
[60] H. Ajiki and T. Ando, J. Phys. Soc. Jpn. **62**, 1255 (1993).
[61] S. Zaric, G. N. Ostojic, J. Kono, J. Shaver, V. C. Moore, M. S. Strano, R. H. Hauge, R. E. Smalley, and X. Wei, Science **304**, 1129 (2004).
[62] U. C. Coskun, T.-C. Wei, S. Vishveshwara, P. M. Goldbart, and A. Bezryadin, Science **304**, 1132 (2004).
[63] B. Lassagne, J.-P. Cleuziou, S. Nanot, W. Escoffier, R. Avriller, S. Roche, L. Forro, B. Raquet, and J.-M. Broto, Phys. Rev. Lett. **98**, 176802 (2007).
[64] M. Bockrath, D. H. Cobden, J. Lu, A. G. Rinzler, R. E. Smalley, L. Balents, and P. L. Mceuen, Nature (London) **397**, 598 (1999).
[65] R. Egger, A. Bachtold, M. S. Fuhrer, M. Bockrath, D. H. Cobden,

and P. L. McEuen, in *Interacting Electrons in Nanostructures*, edited by R. Haug and H. Schoeller, Lecture Notes in Physics Vol. 579 (Springer, Berlin, 2001), p. 125.

[66] H. Ishii, H. Kataura, H. Shiozawa, H. Yoshioka, H. Otsubo, Y. Takayama, T. Miyahara, S. Suzuki, Y. Achiba, M. Nakatake, T. Narimura, M. Higashiguchi, K. Shimada, H. Namatame, and M. Taniguchi, Nature (London) **426**, 540 (2003).

[67] B. Gao, A. Komnik, R. Egger, D. C. Glattli, and A. Bachtold, Phys. Rev. Lett. **92**, 216804 (2004).

[68] J. Lee, S. Eggert, H. Kim, S.-J. Kahng, H. Shinohara, and Y. Kuk, Phys. Rev. Lett. **93**, 166403 (2004).

[69] H.-H. Lin, Phys. Rev. B **58**, 4963 (1998).

[70] T. Giamarchi, *Quantum Physics in One Dimension*, International Series of Monographs on Physics Vol. 121 (Oxford University Press, Oxford, 2004).